Electron-capture, electron-loss, and impact-ionization cross sections for 103- to 3400-keV/amu multicharged iron ions colliding with molecular hydrogen

K. H. Berkner, W. G. Graham,* R. V. Pyle, A. S. Schlachter, and J. W. Stearns
Lawrence Berkeley Laboratory, University of California, Berkeley, California 94720
(Received 15 September 1980)

We report cross-section measurements for collisions of multicharged iron ions with a molecular-hydrogen target: (a) electron capture and electron loss of the multicharged ions, and (b) impact ionization of the hydrogen target. Iron ions, Fe^{+q}, were used with charge states $q = 3$–13 at 103 keV/amu, $q = 9$–16 at 294 keV/amu, $q = 11$–22 at 1160 keV/amu, and $q = 20$–25 at 3400 keV/amu. We find that an empirically determined expression for the electron-capture cross section, $\sigma = (1.2\times10^{-8})\, q^{3.15} E(\text{keV/amu})^{-4.48}$ cm^2/molecule, describes all the data at and above 275 keV/amu. These measurements are compared with recent theoretical calculations.

I. INTRODUCTION

A collision of a multicharged heavy ion X^{+q} with a target atom Y can result in a change of the charge state of the projectile, the target, or both.[1] Cross sections for electron capture,

$$\sigma_{q,q-n}: X^{+q} + Y \rightarrow X^{+(q-n)} + Y^{+n}, \tag{1}$$

and electron loss by the ion,

$$\sigma_{q,q+n}: X^{+q} + Y \rightarrow X^{+(q+n)} + Y + ne, \tag{2}$$

can be determined experimentally by observing the change of the charge state of the projectile.

Cross sections for charge changes of the target Y can be obtained by extracting and analyzing slow collision products.[2] A simpler technique, yielding less information, is to measure total or effective cross sections, σ_+ and σ_-, for producing positive and negative charge in the target. From these, one can deduce a cross section σ_I for the production of charge in the target in excess of that produced by electron capture or loss. This cross section for "impact ionization," which includes contributions from single and multiple ionization of a multielectron target and dissociative ionization of a molecular target, is obtained by subtracting the contribution of electron-capture or electron-loss collisions from the charge production in the target:

$$\sigma_I(q) = \sigma_+(q) - \sum n\sigma_{q,q-n} \tag{3}$$

or

$$\sigma_I(q) = \sigma_-(q) - \sum n\sigma_{q,q+n}. \tag{4}$$

In this paper we report experimental cross sections $\sigma_{q,q-1}$, $\sigma_{q,q+1}$, and σ_I (and in some cases $\sigma_{q,q-2}$ and $\sigma_{q,q+2}$) for collisions of multicharged iron ions, Fe^{+q}, with a molecular-hydrogen target, with $q = 3$–13 at 103 keV/amu, $q = 9$–16 at 294 keV/amu, $q = 11$–22 at 1160 keV/amu, and $q = 20$–25 at 3400 keV/amu. A few of these results have been reported previously.[3–5]

There are extensive review papers on heavy-ion electron capture and loss by Nikolaev[6] and Betz.[7] Published cross-section measurements for electron capture, electron loss, and impact ionization for projectiles heavier than He in H and H_2 targets are listed in Table I.[3–5, 8–37] Electron-capture and electron-loss cross sections for iron ions in H and H_2 have been reported by Meyer *et al.*[24] and Gardner *et al.*[25] at lower energies and charge states than we report here. We are not aware of any previous measurements for impact ionization by iron ions.

Many theoretical techniques have been used to calculate electron-capture, electron-loss, and impact-ionization cross sections for heavy projectiles colliding with atomic hydrogen.

For calculations of electron-capture cross sections the choice of the applicable theoretical model generally depends on how the projectile velocity compares with the orbital velocity of the electron to be captured. In the present paper the projectile velocity is greater than the velocity of the orbiting electron; hence a classical approach can be used in the calculation of electron-capture cross sections. Olson and Salop[38] have used a three-body classical approach, a classical-trajectory Monte Carlo technique, in which all the forces between the three bodies—the projectile, the target, and the captured electron—are included. Molecular effects limit the validity of this approach to energies greater than about 25 keV/amu.[38] At high energies, e.g., 5000 keV/amu, the transition probabilities become so small that the technique is limited by the difficulty in obtaining good statistics for the cross-section determination.

Electron-capture cross sections relevant to the present experiment also have been calculated using quantum-mechanical methods: (1) Rule and Omid-

TABLE I. Summary of published measurements of electron-capture, electron-loss, and impact-ionization cross sections for collisions of heavy projectiles ($Z > 2$) with H and H_2.

Authors	Ref.	Projectiles	Charge states	Targets	Energy range (keV/amu)	Electron capture	Electron loss	Impact Ionization
McCullough *et al.*	8	Ba, Ti, Cd, Zn, Kr, B	2	H, H_2	0.005–8	x		
Nutt *et al.*	9	C, Ti	2	H, H_2	0.01–1.2	x		
Huber and Kahlert	10	Ar, Kr	2–7	H_2	0.012–0.25	x		
Flaks and Ogurtsov	11	N	0–3	H_2	0.07–7	x		x
Sherwin	12	Be, B, C, Al, K, Fe, Cu	1–3	H_2	0.09–0.4	x		x
Muller and Salzborn	13	Ne, Ar, Kr, Xe	2–8	H_2	0.23–1.5	x		
Phaneuf *et al.*	14	C, N, O	1–5	H, H_2	0.5–137	x		
Crandall *et al.*	15	C, N, O	3–6	H_2	0.6–9.2	x		
Crandall *et al.*	16	B, C, N, O, F, Ar	2–8	H, H_2	0.6–9.2	x		
Phaneuf *et al.*	17	N	1–5	H	0.6–18	x		
Gardner *et al.*	18	B, C, N, O	2–5	H	1.0–2.9	x		
Gardner *et al.*	19	B	2–4	H_2	1.1–8.4	x		
Winter *et al.*	20	Ne	1–4	H_2	5		x	x
El-Sherbini *et al.*	21	Ar	6	H_2	5–30		x	x
Shah *et al.*	22	Li	1–3	H, H_2	9–214	x	x	
Goffe *et al.*	23	B, C	1–6	H, H_2	9–200	x	x	
Meyer *et al.*	24	O, Fe, Mo, Ta, W, Au	1–19	H, H_2	24–200		x	
Gardner *et al*	25	Fe	4–13	H, H_2	27–290		x	
Pivovar *et al.*	26	Li	0–3	H_2	28.5–285	x		x
Ryding *et al.*	27	Cl, Br, I	2–7	H_2	32–428	x	x	
Ryding *et al.*	28	I	1–4	H_2	35	x	x	
Betz and Wittkower	29	I	2–18	H_2	39–197	x	x	
Betz *et al.*	30	Br, I	2–10	H_2	47–187	x	x	
Kim *et al.*	31	Si	2–9	H, H_2	51–204	x		
Kim *et al.*	32	Ta, Mo, W, Au	5–18	H	60	x		
Nikolaev *et al.*	33	N	2–4	H_2	80–751	x	x	
Moak *et al.*	34	I	12, 17	H_2	87–1280	x		
Wittkower and Betz	35	I	5	H_2	95	x	x	
Olson *et al*	5	Fe	3–15	H_2	108–290			x
Datz *et al.*	36	Br	6–11	H_2	173–312	x	x	
Berkner *et al.*	4	Fe	9–22	H_2	260–1140	x		x
Berkner *et al.*	3	Fe	20–25	H_2	3400	x	x	
Tonuma *et al.*	37	C, N	4–7	H_2	3500–7500	x	x	

var[39] have used the Oppenheimer-Brinkman-Kramers (OBK) approximation. This technique is known to overestimate the cross sections, but when modified by an empirical factor[40,41] yields cross sections that are consistent with experiments. (2) Chan and Eichler[42] have used the Fock density-matrix expression in momentum space of the target electron to calculate cross sections for electron capture into arbitrary principal shells of energetic bare projectiles. From these results they have derived a scaling factor for cross sections calculated with the OBK method. (3) A unitarized distorted-wave-approximation method, based on traveling atomic orbitals, has been used by Ryufuku and Watanabe.[43] At high energies, their cross sections tend to be twice as large as measured values, but they exhibit the correct charge state and energy dependence.

Electron-loss cross sections for Fe^{+q} in H have been calculated in the first Born approximation, for energies between 0.1 and 100 MeV/amu, by Rule and Omidvar.[39] Calculations of the first Born approximation for the loss of $1s$, $2s$, and $2p$ electrons from hydrogenlike ions in hydrogen have also been reported by Dmitriev *et al.*[44] and Nikolaev *et al.*[45]

Impact-ionization cross sections have been calculated with the three-body classical-trajectory Monte Carlo technique by Olson and Salop[38] and by Olson.[4,5,17] At high energies the plane-wave Born approximation may be more appropriate.[5]

Electron-capture and impact-ionization collisions of multicharged ions with atomic hydrogen (or deuterium) are important for the fusion program. Highly ionized heavy impurity ions, such as Fe^{+25}, Mo^{+33}, and W^{+35}, have been identified in magnetically confined hydrogen plasmas in tokamaks.[46-48] Many of these plasmas are heated by injection of 20 to 120 keV hydrogen or deuterium atoms, and the ionization (trapping) profile of the injected atoms can be altered by the presence of the multicharged impurities.[49] In order to estimate how large an effect the impurity ions could have on the trapping profile, it is necessary to know the cross sections for electron capture,

$$H^0 + A^{+q} \rightarrow H^+ + A^{+(q-1)}, \tag{5}$$

and for impact ionization,

$$H^0 + A^{+q} \rightarrow H^+ + A^{+q} + e^-, \tag{6}$$

where A is an impurity ion in charge state q. The sum of these two cross sections is the total cross section for electron loss from the hydrogen atom.

The results presented here are for molecular-hydrogen targets; we compare these cross sections with twice the theoretical cross sections calculated for an atomic-hydrogen target.

II. EXPERIMENTAL APPROACH

A. General description

The apparatus is shown in Fig. 1. Iron ions of the desired charge state from the SuperHILAC heavy-ion linear accelerator were selected by momentum analysis and passed through the target cell described below.

Two types of measurements were made: (1) impact ionization, in which slow-electron and slow-ion currents in the target were collected with a parallel-plate capacitor, while the fast incident ion beam was measured with a Faraday cup; and (2) charge-transfer measurements, in which the

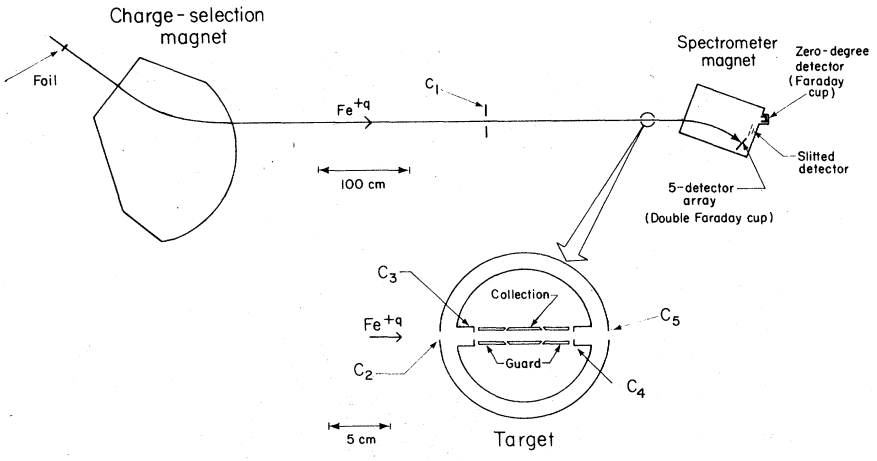

FIG. 1. Schematic diagram of the apparatus. Dimensions of apertures C_1–C_5 are discussed in text.

fast ions exiting the target were analyzed by the spectrometer magnet and detected by an array of diffused-junction solid-state detectors.

B. Preparation of projectile beam

The iron ions from the SuperHILAC were either used directly or stripped further in a carbon foil, which was located upbeam of the charge-state-selection magnet. The foil thickness chosen in each case was a compromise between a thick foil which, at equilibrium thickness, would yield higher charge-state ions, and a thin foil to minimize energy loss in the foil.[50] Since little information exists for charge-state distributions of iron ions in carbon foils, the desired thickness had to be estimated. We used 10 $\mu g/cm^2$ foils for most of the measurements; 100 $\mu g/cm^2$ were used at 3400 keV/amu and for some measurements at 1160 keV/amu. We made no systematic study of the charge-state distribution as a function of beam energy or foil thickness; however, the mean charge state decreased with decreasing beam energy.

Preparation of a fast partially stripped ion beam in a foil can create metastable ions with lifetimes sufficiently long to reach the target. These metastable ions could have different cross sections than ground-state ions, especially for electron loss, since they are less tightly bound than ground-state ions. As we prepared our projectile beams by stripping in a foil, they could contain an unknown admixture of metastable ions.

We used the charge-selection magnet to select ions in a particular charge state from the variety of charge states in the beam emerging from the carbon foil. Charge-state identification and energy measurements are discussed below. In order to ensure a unique path through the charge-selection magnet, a 12-mm-diam aperture was inserted in front of the foil.

Beyond the charge-selection magnet, the beam passed through a 3.2-mm-diam collimator C_1. This collimator and the entrance aperture in the gas-target chamber 178 cm downbeam limited the primary-beam size so that no beam was lost at the target entrance and exit or at the Faraday cup or detectors. Since the exit collimation allowed the scattered beams to be larger than the detectors, the equal widths of the charge-transferred and the primary beams showed that there was negligible beam broadening from scattering. We estimate collimator losses of the charge-transferred beams to be less than 5%; this introduces a possible 5% error in the charge-transfer cross sections. The same loss of primary beam by scattering causes only an estimated 2% error in ionization measurements, since only a small fraction of the primary beam causing the ionization changes charge.

C. Charge-state identification and energy measurement

Considerable care was required to determine the charge state of the primary beam, especially for high charge states, where magnetic separation of adjacent charge states was small.

The spectrometer magnet was calibrated for charge-state identification by a wire-orbit technique, in which a current-carrying wire assumes the path taken by an ion beam of fixed momentum p and charge state q.[51] The wire orbit, defined by collimators C_1, C_2, and a 1.25-mm-wide slit located at the exit of the magnet, was used to obtain the integral of the magnetic field over the path length as a function of the magnetic field measured with a fixed-position Hall probe. A surface barrier detector, mounted behind the slit, was used to determine the p/q ratio of the beam of interest. The beam energy could be determined to within 1% by a reference spectrometer maintained at the superHILAC; we used this measurement to normalize the energy scale for our spectrometer. When this spectrometer was not available, we relied on pulse-height measurements with solid-state detectors.

A complication in the energy determination was the use of a carbon foil to strip ions to higher charge states. The approximate energy loss to be expected in a given foil was obtained from energy-loss tables,[50] and was occasionally checked by measuring the decrease in pulse height on a solid-state detector. We used identical foils in pairs in most of our experiments: one located upbeam of the charge-selection magnet and another foil that could be inserted downbeam of collimator C_1. The latter was used to measure energy loss in the incident beam without the necessity of retuning the charge-selection magnet, thus eliminating the possibility of error in charge-state or energy-loss determination. Once the energy loss in the second foil was determined, we verified that the energy loss in the original foil was comparable; subsequently, only the foil upbeam of the charge-selection magnet was used during the experiment. Corrections for Hall-probe drift and offsets, uncertainties in the wire-orbit calibration, and resolution of the slitted detector lead to a relative standard uncertainty of 1% for measurements taken near a given nominal value. Uncertainties in the relative calibration over a large energy range and in the absolute calibration of the reference spectrometer yield an absolute uncertainty of 3% to 5%. Since the charge-state determination depends on the square root of the energy $\Delta q/q = \Delta E/2E$, we are able to unambiguously determine the charge states of the iron beams.

D. Beam analysis and detection

After passage through the target the beam traversed a 33×61-cm spectrometer magnet (maximum central field 2 T). At zero magnetic field the fast-ion beam could be detected by a 25-mm-diam Faraday cup located on the axis of collimation; secondary electrons were suppressed by a permanent magnet. This Faraday cup was used for tune-up of high-intensity beams; it was replaced by a 25-mm-diam solid-state detector for tune-up of low-intensity beams.

The charge-analyzed beam was detected by either of two methods: a double Faraday cup or an array of solid-state detectors. The double Faraday cup [Fig. 2(a)] consisted of a long rectangular open-ended box ($103 \times 35 \times 25$ mm) which collected all ions that had changed their charge in a collision in the gas target. The primary beam was collected in a small Faraday cup located behind an adjustable slit, typically 7 mm wide, in the rectangular cup. This double Faraday cup was located at the same position as the five-detector array indicated in Fig. 1. Secondary-electron emissions were suppressed in both Faraday cups by the magnetic field of the spectrometer magnet. The currents from the Faraday cups were amplified by electrometers, the outputs of which were integrated.

For measurements of charge-changing cross sections with low-intensity beams, or when simultaneous measurements of single and double electron-capture and electron-loss cross sections were made, the double Faraday cup was replaced with an array of five diffused-junction solid-state detectors [Fig. 2(b)]. Each detector had a sensitive area of 16×10 mm; the detectors were so arranged that each had an exposed area larger than the scattered beam, yet the spacing was such that five beams could be detected simultaneously: the primary beam of charge q, and secondary beams of charges $q+1$, $q+2$, $q-1$, and $q-2$. The entire array was mounted on a sliding shaft so that the position of the array could be changed within the magnet to match the spatial separation of the beams to the detector spacing. For very low values of q, only beams with charges q, $q+1$, and $q-1$ were detected, using the central and the two outer detectors. For each value of q we determined that the detected signals for the various charge states were independent of small changes in the spectrometer magnetic-field settings; this assured that there was no overlapping of adjacent charge-state beams onto neighboring detectors. The signal from each detector was amplified, discriminated, and recorded with a scaler.

The maximum primary-beam intensity was maintained at an average of 10^4 particles/sec; instantaneous count rates were approximately a factor of 100 higher because of the low duty factor of the accelerator. For the primary beam a 100 MHz counting system was used; for the secondary-beam channels 1 MHz counting systems were used. Periodic checks were made to verify that cross sections were independent of counting rate up to the maximum rate used for each measurement.

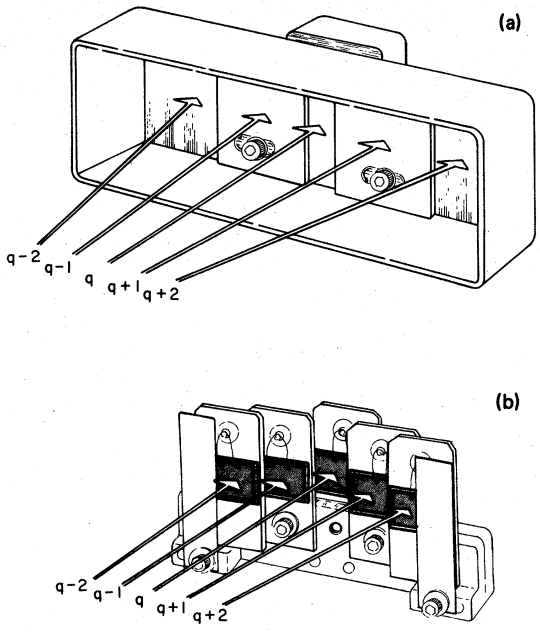

FIG. 2. (a) Schematic diagram of Faraday-cup assembly. (b) Schematic diagram of solid-state-detector array.

E. Target

The gas cell was a differentially pumped chamber with an inner diameter of 7.5 cm, and with entrance and exit apertures (C_3 and C_4) of 3.3 mm diameter (Fig. 1). Apertures C_2 and C_5 had diameters of 2.5 and 3.8 mm and served to isolate the differentially pumped section from the beam line. Apertures C_1 and C_2 limited the beam incident on the target to a half-angle divergence of 0.093° and a beam diameter at the detectors of 6.6 mm. Some measurements were made with a slightly different geometery described in Ref. 4.

A set of parallel plates (Fig. 1 inset) inside the gas cell was used for measuring impact-ionization cross sections by collecting slow ions and slow electrons. The plates were 3.00 cm long, 1 cm apart, and had guard plates on each end to provide a uniform transverse electric field. Slow ions and electrons produced by impact-ionization or charge-changing collisions were swept from a

well-defined length of the target chamber by the electric field and collected on one of the plates. The electric field was increased until the collected currents were insensitive to further changes; the typical field was 120 V/cm. The measurements required incident beams of sufficient intensity that current-measuring techniques could be used. Currents collected at the plates were detected with electrometers, the outputs of which were integrated. Secondary-electron emission from the collecting plates is discussed in Sec. II F.

The pressure in the gas cell was measured with a differential capacitance manometer whose calibration was checked, at high pressures, with an oil manometer. The uncertainty in this measurement is ±4%; the uncertainty in the gas-cell length and variations in ambient temperature are less than 2%, leading to an overall target-thickness uncertainty of 4%. One gas sample was analyzed for impurities and was found to contain 0.06% N_2. From limited measurements with N_2 and Ar targets, we estimated the effect of this N_2 admixture to be 10% for ionization cross sections and 3% for electron-capture cross sections. It is included as a source of uncertainty in Sec. II H.

Charge-transfer collisions in background gas reduce the charge-state purity of the primary beam, especially at low energies. It was therefore found necessary to maintain the pressure in the beam-line between the charge-selection magnet and the gas-target cell below 10^{-6} Torr at maximum gas-cell thickness, while the pressure in the spectrometer magnet was kept below 2×10^{-6} Torr. The spectrometer magnet permitted us to verify that the incident-beam charge-state purity was better than 99%.

F. Electron emission from ion collector

The condenser-plate method of collecting slow-ion and slow-electron current in the target is potentially inaccurate due to the possibility that the slow ions will produce emission of electrons from the ion-collector surface; these secondary electrons will be swept by the electric field in the target and will be collected at the electron collector. This effect increases the apparent current at each electrode and, if not accounted for, produces a corresponding error in the cross section being measured. We determined the magnitude of this effect in a separate experiment on a small accelerator, using the same target chamber, but with the addition of a solenoidal magnetic field coaxial with the beam to suppress secondary electrons.

A 120–150-keV D^+ beam was passed through the target chamber to produce the slow ions, and the beam-normalized ion-collector current was monitored while varying the transverse electric field, the axial magnetic field, and the target pressure. The secondary electrons were considered to be suppressed when a change in the magnetic field produced no change in the normalized ion-collector current. At 100 V/cm a field of about 200 G was required to suppress electrons. With H_2 as the target gas, electron emission represents less than 2% of the pressure-dependent slow-ion current.

G. Data acquisition and analysis: electron-capture and electron-loss cross sections

The slow-ion and slow-electron collection plates were grounded for charge-transfer cross-section measurements. A beam in charge state q was selected by the charge-selection magnet and its charge state was verified by deflecting it onto the slitted detector in the spectrometer magnet. The primary beam was then centered on the middle detector of the five-detector array. The correct spacing of the detectors was confirmed by observing that, with gas in the cell to produce charge-changed ions, the detector signals were independent of small variations in the analyzer field.

A measurement consisted of counting pulses from the five detectors for a time sufficient to achieve reasonable statistics; typical counting times were one minute. Each cross-section measurement consisted of at least ten such measurements at various pressures. Typical data are shown in Fig. 3. Because of the long integration times we had to consider possible variations in the target pressure. Therefore, either the pressure was read during the middle of the counting period or the output from the manometer was integrated throughout the counting period and then divided by the integration time, to average small pressure drifts. We were not always able to determine all four charge-transfer cross sections, either because some were too small to measure in a reasonable integration time, or because of background effects. Background was important for two-electron-transfer cross-section measurements: the primary beam was prepared in charge state q, but collisions with background gas before reaching the target could contaminate this beam with an admixture of ions in charge states $q \pm 1$. A single collision of an ion in charge state $q \pm 1$ in the target then could give an ion in charge state $q \pm 2$, which could mask the single-step, two-electron-transfer cross section that was to be measured.

We also measured a few charge-transfer cross sections with the Faraday-cup array: The primary beam was collected on the small cup, secondary beams (electron capture or loss) on the large cup. This technique required higher intensity beams

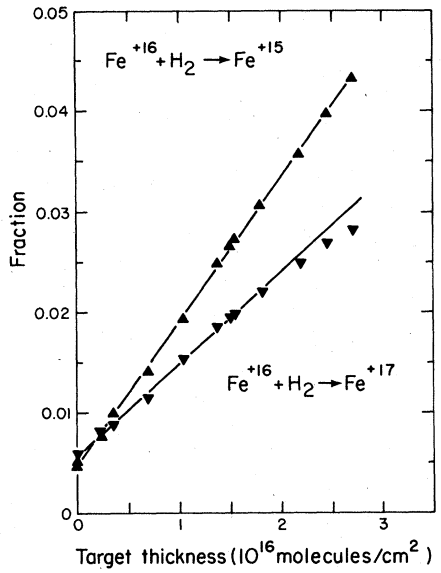

FIG. 3. Charge-state fractions F_{15}(▲) and F_{17}(▼) as a function of target thickness, for 1160 keV/amu Fe^{+16} in H_2. Lines are solutions of a least-squares fit to the data (including corrections for second-order effects) from which the cross sections were obtained [Eq. (9)]. The F_{15} and F_{17} fractions were used to determine, respectively, the single-electron-capture and single-electron-loss cross sections.

and could be used only when one of the cross sections (either single-electron capture or loss) dominated. The dominant reaction could be determined by sweeping the secondary beams across the small cup. Several cross sections were measured with the solid-state detectors and with the Faraday-cup array. The results agreed within the estimated uncertainties.

The population of a charge state k, expressed as a fraction of the total beam F_k is related to the target thickness π (the target density times path length through target) by coupled equations

$$\frac{dF_k}{d\pi} = \sum_{j\neq k} (F_j\sigma_{j,k} - F_k\sigma_{k,j}), \tag{7}$$

where $\sigma_{j,k}$ is the cross section for changing the beam ion from charge state j to charge state k. Complete solutions to these equations for a three-level system are listed in articles by Allison and Garcia-Munoz.[52]

An initial approximation for the single-electron-capture and single-electron-loss cross sections is obtained using the thin-target approximation or first-order expansion of Eq. (7). For an incident beam in charge state j, we have

$$\sigma_{j,j\pm1} = \frac{\Delta F_{j\pm1}}{\Delta\pi}. \tag{8}$$

We have used this expression for those results for which the beam attenuation was less than 10%, so that errors in σ due to attenuation were less than 5%.

These first-order solutions were used in a second-order expansion of Eq. (7), which can be written as

$$\pi\sigma_{j,k} = \frac{2}{F_j+1}F_k - \frac{\pi}{2}\sum_{(k\pm1)\neq j} F_{k\pm1}\sigma_{k\pm1,k} + \frac{\pi}{2}\sum_{(k\pm1)\neq j} F_k\sigma_{k,k\pm1}. \tag{9}$$

The factor applied to F_k is the "attenuation" correction and the other terms are the "two-step" corrections. The effect of this approximation is to linearize the data within the region of the thin-target definition. The final cross-section results were obtained from the slope of a least-squares fit of the expression on the right-hand side of Eq. (9).

H. Data acquisition and analysis: impact-ionization cross sections

An ion beam in charge state q was selected by the charge-selection magnet and its charge state was verified by deflecting it onto the slitted detector in the spectrometer magnet. The small cup of the double Faraday-cup assembly was used to measure the primary beam, while beam attenuation was monitored by measuring the fraction of the beam in the large cup. The voltage on the collector plates was varied until the slow-ion and slow-electron currents, I^+ and I^-, did not change with further increases of voltage. Figure 4 shows a typical collector voltage sweep. (At this energy, charge transfer is much smaller than ionization,

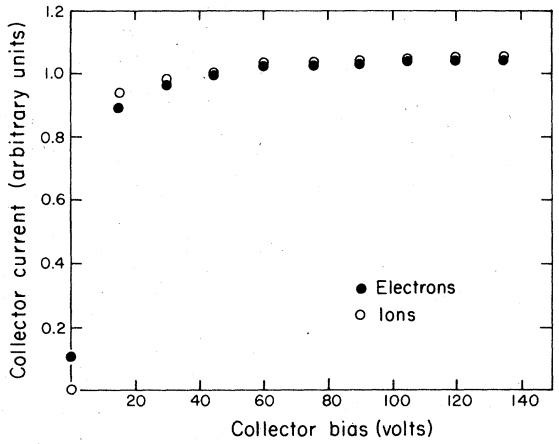

FIG. 4. Slow-ion and slow-electron current (arbitrary units) to collector plates in target, as a function of bias voltage applied to the plates, for 1160 keV/amu Fe^{+16} incident on H_2.

hence $\sigma_+ \approx \sigma_- \approx \sigma_I$.) Operating voltages were about 120 V. Once this operating voltage was determined, simultaneous measurements were made of collected slow-ion or slow-electron current, primary-beam current (small cup), and charge-transferred beam current (large cup). The electrometer outputs were integrated for 30 to 60 sec, a time long compared to the time constant of the electrometers. Primary-beam currents of 10^{-8} A to 10^{-13} A were used to make these measurements. A measurement consisted of the integrated output of the three electrometers and the average pressure. We made measurements at more than ten different pressures to obtain a cross section. Typical data are shown in Fig. 5.

Secondary electrons from the double Faraday cup were suppressed by the spectrometer-magnet field. Secondary-electron emission from the ion-collection plates has been discussed in Sec. II F. The electrometers were calibrated against a secondary current standard.

Over a pressure range in which primary-beam attenuation and ionization (by electrons produced in the target) were both small (thin target), our initial approximation for the cross section for electron production by Fe^{+q} was

$$\sigma_-(q) = \frac{\Delta F_-(q)}{\Delta \pi}, \tag{10}$$

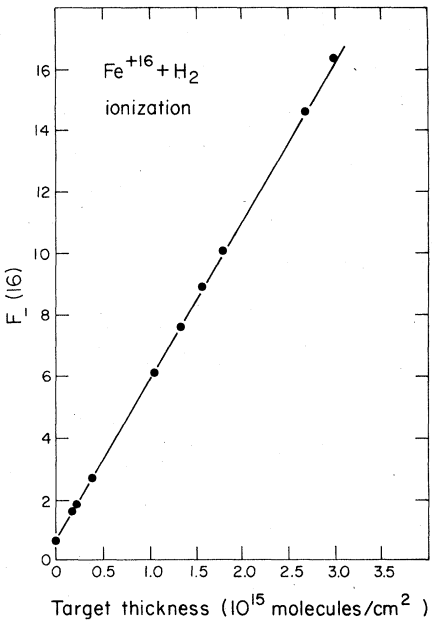

FIG. 5. Fraction $F_-(16)$ of slow electrons produced in target as a function of target thickness for 1160 keV/amu Fe^{+16} in H_2. Line is solution of a least-squares fit to the data (including corrections for second-order effects) from which the ionization cross section was obtained [Eq. (12)].

where F_- is the number of electrons produced in the target per primary particle, and I_q is the primary-beam current

$$F_-(q) = \frac{I^-}{(I_q/q)}. \tag{11}$$

Equation (10) was used to obtain an initial approximation of electron-production cross sections for beams of different charge states. Second-order corrections were made to linearize the data

$$\pi\sigma_-(q) = \frac{F_-(q) - a\frac{\pi^2}{2}\left[\sigma_{q,q-1}\sigma_-(q-1) + \sigma_{q,q+1}\sigma_-(q+1)\right]}{(1+F_q)/2}, \tag{12}$$

where q is the incident charge state, F_q is the fraction of the beam remaining in that charge state (either measured or estimated from the cross sections), and a is the ratio of the total gas-cell length to the length of the collector region. The two subtractive terms in the numerator remove, to first order, the charge produced by the incident beam admixture in adjacent charge states, while the divisor corrects for attenuation of the primary beam. The slope of a least-squares fit to the right-hand expression was used to determine $\sigma_-(q)$.

Similarly, the cross section for the production of slow ions is, to first order,

$$\sigma_+(q) = \frac{\Delta F_+(q)}{\Delta \pi}, \tag{13}$$

where the definition of F_+ is analogous to Eq. (11). The second-order corrections were made with an equation analogous to Eq. (12).

Since electron capture and loss by the primary beam can also create charge in the target, the impact-ionization cross section $\sigma_I(q)$ is

$$\begin{aligned}\sigma_I(q) &= \sigma_+(q) - \sigma_{q,q-1} \\ &= \sigma_-(q) - \sigma_{q,q+1}.\end{aligned} \tag{14}$$

Values of σ_I obtained from either σ_+ or σ_- agreed within 2%.

I. Uncertainties

The relative standard uncertainty in our single-electron-capture and single-electron-loss cross sections is estimated to be 4%. This is obtained from uncertainties in the least-squares fit (3%) (which averages contributions from counting statistics, zero drift in the capacitance manometer, and corrections for second-order processes), from counting errors due to intensity fluctuations in the beam (2%), and from possible beam-energy drift during a sequence of measurements (2%). The cross sections for two-electron capture and

loss are less certain because of corrections for two-step processes and poor counting statistics, and the estimated relative standard uncertainties are 10%. For possible systematic errors we estimate 4% for the determination of the target thickness (calibration of the capacitance manometer and determination of the length of the gas cell), 5% for possible beam loss on collimators, and 3% due to gas impurities; the systematic error is thus estimated to be 7%. Combining the relative and systematic uncertainties, we obtain an absolute standard uncertainty of 8% for the single-electron-capture and single-electron-loss cross sections and 12% for the two-electron-capture and two-electron-loss cross sections.

The ionization cross sections have the following sources of relative uncertainty: zero drift and fluctuations in electrometers and in the capacitance manometer (3%), corrections for second-order processes (2%), scale-to-scale variations in the electrometer-integrator system (3%), correction for secondary-electron emission from the collector plates (2%), and uncertainty in the slow ion/electron collection efficiency (5%). The total standard relative uncertainty is 7%. The estimates of systematic errors are as follows: target thickness (4%), beam loss on collimators (2%), gas impurity (1%), and differences in using σ_+ or σ_- for the determination of σ_I (2%); the systematic error is thus estimated to be 5%. Combining the relative and systematic uncertainties, we estimate an absolute standard uncertainty of 8% for the ionization cross sections.

III. RESULTS AND DISCUSSION

A. Projectile electron capture

Our electron-capture cross-section results for Fe^{+q} projectiles in an H_2 target are given in Table II. The two-electron double-capture cross sections were often masked by competing two-step processes or poor counting statistics.

The single-electron-capture cross sections $\sigma_{q,q-1}$ vs charge state q are shown in Fig. 6. From the figure it is clear that the cross sections have a strong energy dependence, and, at a given energy, the cross sections exhibit a power-law dependence with q. In an attempt to find a general expression for the energy and charge-state dependence of the single-electron-capture cross sections, we chose a power-law expression of the form

$$\sigma_{q,q-1}(q,E)=\sigma_a q^{\alpha}E^{\beta}, \tag{15}$$

where σ_a, α, and β are constants. There are no values for σ_a, α, and β for which Eq. (15) describes all our results; however, our results at 275 keV/amu and above are in excellent agreement with the expression

$$\sigma_{q,q-1}(q,E)=(1.2\times10^{-8})q^{3.15}E^{-4.48}, \tag{16}$$

where $\sigma_{q,q-1}$ is the cross section in cm^2 and E is the projectile energy in keV/amu. To demonstrate the range over which Eq. (16) describes the data, we have plotted $q^{-3.15}\,\sigma_{q,q-1}$ vs E in Fig. 7(a) and $E^{4.48}\,\sigma_{q,q-1}$ vs q in Fig. 7(b). We also show the scaled cross sections for Fe^{+q} in H_2 from Gardner *et al.*[25] and Meyer *et al.*[24]

At energies greater than 275 keV/amu, $\sigma_{q,q-1}$ fit Eq. (16), while cross sections at lower energies deviate increasingly with decreasing energy. Our results for $\sigma_{q,q-1}$ for Fe^{+q} in H_2 are also in good agreement with previously reported values.[24,25]

Other authors have observed a discontinuity in the electron-capture q scaling at values of q corresponding to closed shells.[29,30,36,53] Gardner *et al.*[25] observed such a discontinuity for electron capture by Fe^{+q} in H, H_2, and Ar targets for Fe^{+8}, which is argonlike. We see no discontinuity in our cross sections at $q=8$ (argonlike), $q=16$ (neonlike), or $q=24$ (heliumlike).

We compare our experimental results for electron capture by Fe^{+q} in H_2 with theoretical calculations for Fe^{+q} in H in Fig. 8, where we have doubled the theoretical results for comparison with molecular hydrogen. The modified OBK calculations by Rule and Omidvar[39] and by Chan and Eichler[42] are in very good agreement with our results above 1000 keV/amu. Chan and Eichler have also calculated cross sections at lower energies, but the agreement gets progressively worse as the energy decreases. The results of Ryufuku and Watanabe[43] are about twice as large as our measured values over the entire energy range. The classical-trajectory Monte Carlo results of Olson[4] are within ±50% of our measurements at 102 and 294 keV/amu. All of the calculations predict a charge-state variation consistent with our results.

B. Projectile electron loss

Our electron-loss cross sections are given in Table II. Two-electron-loss cross sections were masked by competing two-step processes or poor counting statistics except at 3400 keV/amu. We are not aware of any previous electron-loss cross-section measurements for Fe^{+q} projectiles.

The single-electron-loss cross sections $\sigma_{q,q+1}$ vs charge state q are shown in Fig. 9. The cross sections have a weak energy dependence over the range reported here and decrease rapidly with increasing q. It is clear from the figure that there is no simple power-law scaling to describe the q dependence. Previous measurements[27] with other projectiles with lower q's and lower energies have

TABLE II. Electron-capture, electron-loss, and impact-ionization cross sections. Fe^{+q} in H_2. All units in 10^{-16} cm^2/molecule. Random standard uncertainties are ±5% unless otherwise indicated. Systematic uncertainties add an additional ±7% to absolute magnitudes (see Sec. II H).

Energy (MeV)	keV/amu	Charge state	$\sigma_{q,q-1}$	$\sigma_{q,q-2}$	$\sigma_{q,q+1}$	$\sigma_{q,q+2}$	σ_I
190 ± 9	3400	25	0.000 39		0.000 003 4[d]		
		24	0.000 36		0.000 01[b]		
		23	0.000 30[a]		0.000 29		
		22	0.000 28[b]		0.000 64[a]	0.000 004 3[d]	
		21	0.000 25[a]		0.001 0	0.000 018[b]	
		20	0.000 23[a]		0.001 7		
65.0 ± 1.9	1160	22	0.043 0	0.000 39[a]	0.000 34[a]		95.0
		20	0.031 5	0.000 14[b]	0.001 2[a]		74.0
		18	0.025 0	0.000 25[a]	0.003 8		63.0
		16	0.014 2	0.000 06[d]	0.009 0	0.000 06[d]	51.0
		14	0.010 8		0.022	0.002 3 [a]	43.5
		13					38.5
		12	0.006 4		0.040		35.5
		11					33.0
60.0 ± 1.8	1070	21	0.051	0.005[a]	0.000 7[b]		
		20	0.045		0.000 85[d]		
16.5 ± 0.7	294	16	5.6[a]				
		15					83[a]
		14	4.4				81
		13					76
		12	2.8				71
		11					65
		10	1.3				59
15.8 ± 0.5	282	9	1.21		0.10[b]		48.5
15.4 ± 0.5	275	14	5.70	0.30[c]			
		12	3.3	0.16[c]			
6.16 ± 0.29	110	3	0.65		1.13		14.9
5.77 ± 0.28	103	13	43.6				
		11	31.6				50[a]
		9	18.9				44[a]
		7	11.3				36[a]

[a] ±10% uncertainty.
[b] ±15% uncertainty.
[c] ±20% uncertainty.
[d] ±30% uncertainty.

been consistent with cross sections that scale as $q^{-\alpha}$, where α ranges between 2 and 3; we find that for $q \geq 10$, α ranges between 9 and 12.

A notable feature in the single-electron-loss cross sections is the pronounced discontinuity between projectiles with $q = 23$ (lithiumlike) and $q = 24$ (heliumlike). This can be attributed to the shell structure of the iron ion: The energy necessary to ionize Fe^{+25} ($1s$) or Fe^{+24} ($1s^2$) is 9.0 and 8.5 keV, respectively. The energy required to ionize Fe^{+23} ($1s^2 2s$), Fe^{+22} ($1s^2 2s^2$), Fe^{+21} ($1s^2 2s^2 2p$), etc., is 2.0 keV or less.[54] Thus the large discontinuity in electron loss is a clear manifestation of the shell structure of Fe. We might also expect that $\sigma_{24,25}$ would be approximately twice $\sigma_{25,26}$, since there are two $1s$ electrons to be removed from Fe^{+24}, while only one from Fe^{+25}; we observe cross sections with approximately this behavior.

Also shown in Fig. 9 are the first-Born-approximation results of Rule and Omidvar[39]; the agreement is within the experimental uncertainties. There is also good agreement with the calculations of Dmitriev *et al.*[44] for Fe^{+25}. For $q = 20$–23 our cross sections are only 5–20% higher than those calculated by Nikolaev *et al.*,[45] but for Fe^{+24} our results are 30% larger than calculated. Nikolaev[55] suggests that this could be attributed to a metastable contamination of about 1%.

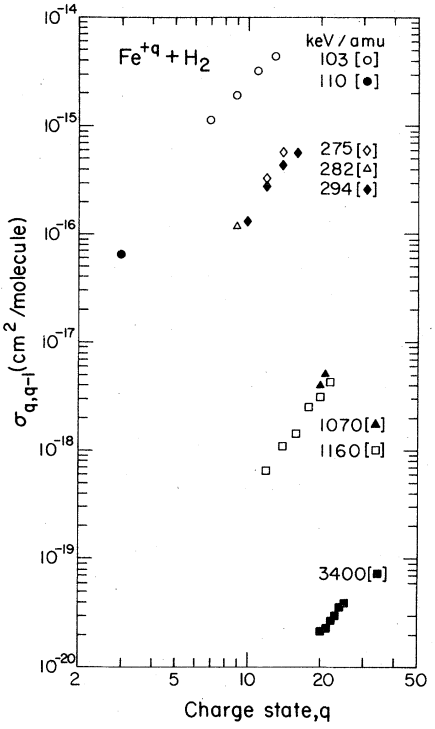

FIG. 6. Single-electron-capture cross sections $\sigma_{q,q-1}$ vs q, for Fe^{+q} in H_2: results of present experiment. Projectile energies are identified by symbols.

C. Target impact ionization

Impact-ionization cross sections for Fe^{+q} in H_2 are shown in Fig. 10. The impact-ionization cross sections are not monotonic with energy; there is a maximum in the ionization cross section at a few hundred keV/amu. Olson[4] has used the classical-trajectory Monte Carlo method to calculate impact-ionization cross sections for Fe^{+q} in atomic hydrogen. Calculated cross sections have been multiplied by a factor of 2 for comparison with our experimental results for H_2. There is very good agreement at 1160 and 294 keV/amu. At 103 keV/amu the agreement in magnitude between theory and experiment is poor, which may mean that the description of the H_2 molecule as two H atoms becomes increasingly invalid as the collision velocities decrease and approach those of the molecular regime.

At high velocities, calculations based upon the Born-binary encounter,[56] or semiclassical approximation, predict a q^2 dependence for the impact-ionization cross section. At our highest energy the ionization cross section has a $q^{1.43\pm0.05}$ dependence. These methods are of use in the present energy range only for collisions of light projectiles and so are not applicable to the present results.

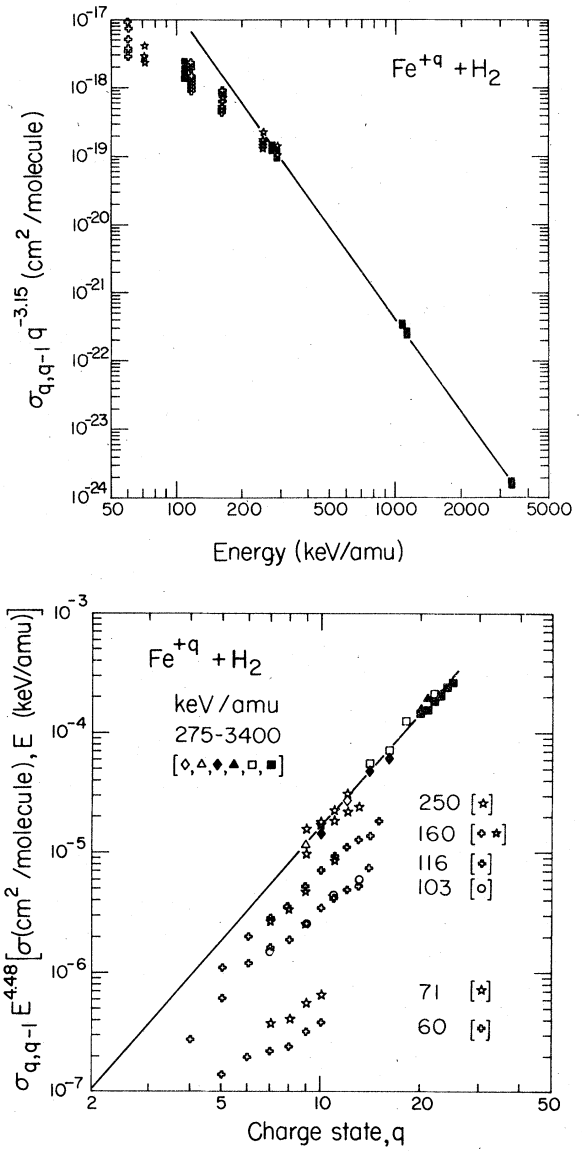

FIG. 7. Single-electron-capture cross sections $\sigma_{q,q-1}$ scaled empirically to the form $\sigma = (1.2\times10^{-8}) q^{3.15} E^{-4.48}$ (solid line), for Fe^{+q} in H_2. (a) Energy dependence of $\sigma_{q,q-1}$, scaled by $q^{-3.15}$. Symbols: ■, present experiment; ✣, Meyer *et al.* (Ref. 24); ★, Gardner *et al.* (Ref. 25). (b) Charge-state dependence of $\sigma_{q,q-1}$, scaled by $E^{4.48}$. The present experimental results are shown using the same symbols as in Figs. 6 and 7(a).

D. Target electron loss

The total cross section for loss of an electron from a hydrogen target is the sum of the electron-capture cross section and the impact-ionization cross section. From the measurements shown in Figs. 6 and 10 we can compute the H_2-target electron-loss cross section for Fe^{+q} projectiles with

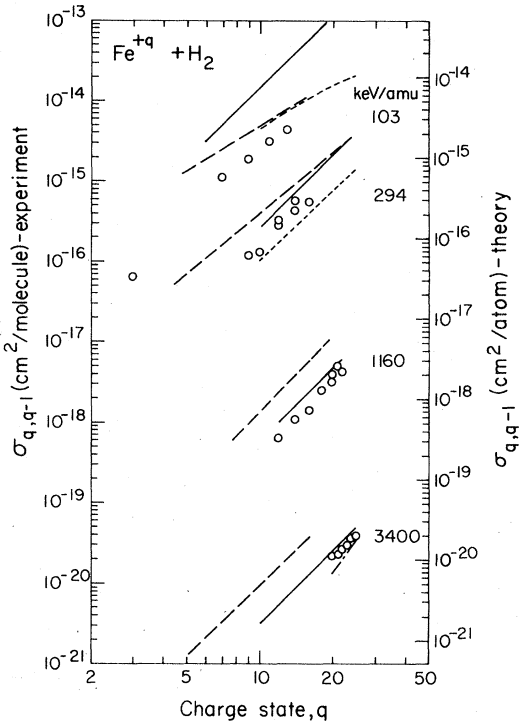

FIG. 8. Single-electron-capture cross sections $\sigma_{q,q-1}$ for $Fe^{+q} + H_2$ (experiment, left ordinate) and $Fe^{+q} + H$ (theory, right ordinate). Short-dashed line is the classical-trajectory calculation of Olson (Ref. 5); solid line, the modified OBK calculation of Chan and Eichler (Ref. 42); long-dashed line, the UDWA calculation of Ryufuku and Watanabe (Ref. 43); and the dot-dashed line, the modified OBK calculation of Rule and Omidvar (Ref. 39).

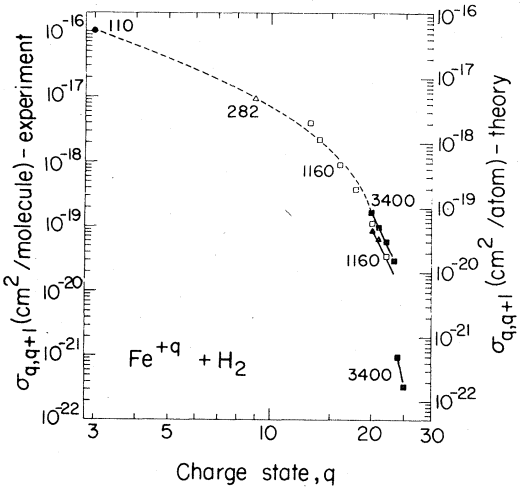

FIG. 9. Single-electron-loss cross sections $\sigma_{q,q+1}$ for $Fe^{+q} + H_2$ (experiment, left ordinate) and $Fe^{+q} + H$ (theory, right ordinate). Present results: ●, 110 keV/amu; △, 282 keV/amu; ▲, 1070 keV/amu; □, 1160 keV/amu; ■, 3400 keV/amu. Solid lines are calculations by Rule and Omidvar (Ref. 39); dashed line is only to guide the eye.

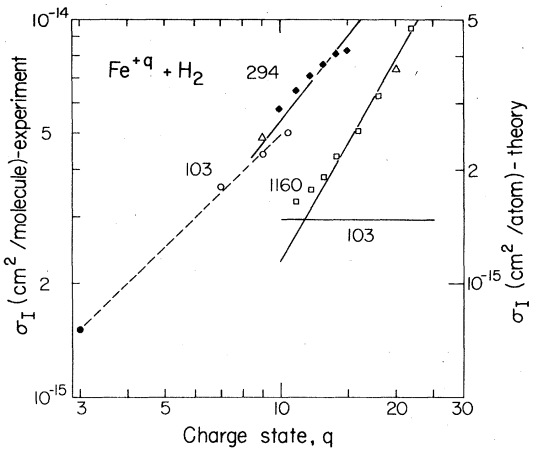

FIG. 10. Impact-ionization cross sections σ_I for $Fe^{+q} + H_2$ (experiment, left ordinate) and $Fe^{+q} + H$ (theory, right ordinate). Symbols are same as in Figs. 6 and 9. Numbers indicate energy in keV/amu. Solid lines are classical-trajectory calculations of Olson (Ref. 5). Dashed line visually connects experimental point $q = 3$ with the 103 keV/amu experimental points at higher q values.

$q = 11$–22 at 1160 keV/amu, $q = 9$–16 at 294 keV/amu, and $q = 3$–13 at 103 keV/amu. These measurements are found to be in excellent agreement with the classical-trajectory calculations of Olson.[5] We have previously reported that the electron-loss cross sections can be combined into a universal scaling rule, applicable for a very wide range of projectile energies and charge states[5]; we found that these results could be fitted to an analytic expression of the form

$$\sigma_{loss} = 4.6 \times q \times 10^{-16}(32q/E) \times [1 - \exp(-E/32q)], \quad (17)$$

where σ_{loss} is the H-atom electron-loss cross section in cm^2, q is the ion charge state, and E is the energy in keV/amu. This equation is valid for $1 \leq q \leq 50$ and for energies in the range 50–5000 keV/amu. The present cross sections are compared with Eq. (17) and with the plane-wave Born-approximation cross section for ionization only[57,58] in Fig. 11.

IV. CONCLUSION

We have measured electron-capture, electron-loss, and impact-ionization cross sections for highly stripped iron ions in an H_2 target. Electron-capture cross sections are found to obey an empirical scaling rule in energy/nucleon, E, and charge state q, for energies greater than 275 keV/amu; the cross sections are proportional to $E^{-4.48} q^{3.15}$.

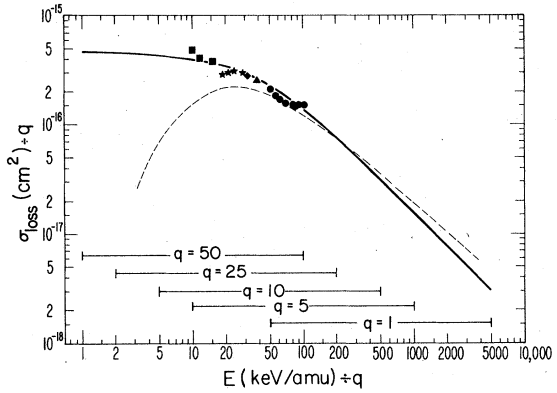

FIG. 11. Hydrogen electron-loss cross section. Solid line: calculated cross section σ_{loss} for electron loss by atomic H in collision with an ion in charge state q; valid for $1 \leq q \leq 50$ and for energies in range 50–5000 keV/amu (Ref. 5). Range of E/q values for which curve is valid is indicated by bars below curves. Uncertainty in the calculated cross sections is ± 25%. Dashed line: plane-wave Born-approximation cross section for ionization only (Refs. 57 and 58). Symbols: Present experimental results for $Fe^{+q} + H_2$ divided by a number between 1.5 and 2.0 to allow comparison with the calculations (see discussion in Ref. 5). Uncertainty is ± 30%. ■, 103 keV/amu, q =7–11; ▲, 110 keV/amu, q =3; ◆, 282 keV/amu, q =9; ★, 294 keV/amu, q =10–15; ●, 1160 keV/amu, q =11–22.

We have compared our cross sections measured in H_2 with twice the theoretical cross sections calculated for an H target, and found good agreement with modified OBK calculations at high energies.

We have found electron-loss cross sections in H_2 to be a slow function of energy, but to decrease rapidly with projectile charge state. We also have found a pronounced discontinuity in electron loss, attributable to the shell structure of the Fe projectile. There is good agreement with calculations by Rule and Omidvar, by Dimitriev *et al.*, and by Nikolaev *et al.* for an H target, multiplied by 2.

Impact-ionization cross sections are in excellent agreement with classical-trajectory Monte Carlo calculations of Olson, except at the lowest energy, where molecular effects make comparison of cross sections for H and H_2 questionable. It would be very desirable to measure ionization cross sections for heavy multiply charged ions colliding with atomic hydrogen.

Our results are consistent with a scaling rule based on CTMC calculations for electron loss from H in collision with a highly stripped ion, valid for a wide range of energies and charge states. We have recently found[59] a scaling rule of similar form for ionization of rare-gas targets.

ACKNOWLEDGMENTS

We would like to thank Dr. M. I. Green and D. H. Nelson for their advice and assistance in the wire-orbit calibration of the spectrometer magnet, R. R. Stevenson for helpful discussions about SuperHILAC operations, and L. A. Biagi, H. H. Hughes, J. R. Meneghetti, and members of their groups for skillful technical assistance. We would like to thank Dr. R. E. Olson for many enlightening discussions, and Professor C. L. Cocke for helpful suggestions. We also thank Professor J. E. Bayfield for providing us with unpublished results and a copy of Dr. L. D. Gardner's thesis. This work was supported by the Fusion Energy Division of the U. S. Department of Energy under Contract No. W-7405-ENG-48.

*Present address: The New University of Ulster, Coleraine, BT52 1SA, N. Ireland.

[1]R. E. Olson, in *Electronic and Atomic Collisions*, edited by N. Oda and K. Takayanagi (North-Holland, New York, 1980), pp. 391–405. For a general description of experimental techniques, see H. Tawara and A. Russek, Rev. Mod. Phys. 45, 178 (1973).

[2]N. V. Fedorenko and V. V. Afrosimov, Zh. Tekh. Fiz. 26, 1938 (1956) [Sov. Phys.—Tech. Phys. 1, 1872 (1956)].

[3]K. H. Berkner, W. G. Graham, R. V. Pyle, A. S. Schlachter, and J. W. Stearns, Phys. Lett. 62A, 407 (1977).

[4]K. H. Berkner, W. G. Graham, R. V. Pyle, A. S. Schlachter, J. W. Stearns, and R. E. Olson, J. Phys. B 11, 875 (1978).

[5]R. E. Olson, K. H. Berkner, W. G. Graham, R. V. Pyle, A. S. Schlachter, and J. W. Stearns, Phys. Rev. Lett. 41, 163 (1978).

[6]V. S. Nikolaev, Usp. Fiz. Nauk 85, 679 (1965) [Sov. Phys. Usp. 8, 269 (1965)].

[7]H. D. Betz, Rev. Mod. Phys. 44, 465 (1972).

[8]R. W. McCullough, W. L. Nutt, and H. B. Gilbody, J. Phys. B 12, 4159 (1979).

[9]W. L. Nutt, R. W. McCullough, and H. B. Gilbody, J. Phys. B 11, L181 (1978).

[10]B. A. Huber and H. J. Kahlert, J. Phys. B 13, L159 (1980).

[11]I. P. Flaks and G. N. Ogurtsov, Zh. Tekh. Fiz. 33, 748 (1963) [Sov. Phys.—Tech. Phys. 8, 560 (1963)].

[12]C. W. Sherwin, Phys. Rev. 57, 814 (1940).

[13]A. Müller and E. Salzborn, Inst. Phys. Conf. Ser. No. 38, 169 (1978).

[14]R. A. Phaneuf, F. W. Meyer, and R. H. McKnight, Phys. Rev. A 17, 534 (1978).

[15]D. H. Crandall, M. L. Mallory, and D. C. Kocher, Phys. Rev. A 15, 61 (1977).

[16]D. H. Crandall, R. A. Phaneuf, and F. W. Meyer,

Phys. Rev. A 19, 504 (1979).
[17]R. A. Phaneuf, F. E. Meyer, R. H. McKnight, R. E. Olson, and A. Salop, J. Phys. B 10, L425 (1977).
[18]L. D. Gardner, J. E. Bayfield, P. M. Koch, I. A. Sellin, D. J. Pegg, R. S. Peterson, and D. H. Crandall, Phys. Rev. A 21, 1397 (1980).
[19]L. D. Gardner, J. E. Bayfield, P. M. Koch, I. A. Sellin, D. J. Pegg, R. S. Peterson, M. L. Mallory, and D. H. Crandall, Phys. Rev. A 20, 766 (1979).
[20]H. Winter, E. Bloemen, and F. J. de Heer, J. Phys. B 10, L453 (1977).
[21]Th. M. El-Sherbini, A. Salop, I. Bloemen, and F. J. de Heer, J. Phys. B. 13, 1433 (1980).
[22]M. B. Shah, T. V. Goffe, and H. B. Gilbody, J. Phys. B 11, L233 (1978).
[23]T. V. Goffe, M. B. Shah, and H. B. Gilbody, J. Phys. B 12, 3763 (1979).
[24]F. W. Meyer, R. A. Phaneuf, H. J. Kim, P. Hvelplund, and P. H. Stelson, Phys. Rev. A 19, 515 (1979).
[25]L. D. Gardner, J. E. Bayfield, P. M. Koch, H. J. Kim, and P. H. Stelson, Phys. Rev. A 16, 1415 (1977); L. D. Gardner, Ph.D. thesis, University of Pittsburg, 1978 (unpublished).
[26]L. I. Pivovar, Yu. Z. Levchenko, and G. A. Krivonosov, Zh. Eksp. Teor. Fiz. 59, 19 (1970) [Sov. Phys.—JETP 32, 11 (1971)].
[27]G. Ryding, H. D. Betz, and A. Wittkower, Phys. Rev. Lett. 24, 123 (1970).
[28]G. Ryding, A. Wittkower, and P. H. Rose, Phys. Rev. 184, 93 (1969).
[29]H. D. Betz and A. B. Wittkower, Phys. Rev. A 6, 1485 (1972).
[30]H. D. Betz, G. Ryding, and A. B. Wittkower, Phys. Rev. A 3, 197 (1971).
[31]H. J. Kim, R. A. Phaneuf, F. W. Meyer, and P. H. Stelson, Phys. Rev. A 17, 854 (1978).
[32]H. J. Kim, P. Hvelplund, F. W. Meyer, R. A. Phaneuf, P. H. Stelson, and C. Bottcher, Phys. Rev. Lett. 40, 1635 (1978).
[33]V. S. Nikolaev, L. N. Fateeva, I. S. Dmitriev, and Ya. A. Teplova, Zh. Eksp. Teor. Fiz. 33, 306 (1957) [Sov. Phys.—JETP 6, 239 (1958)].
[34]C. D. Moak, H. O. Lutz, L. D. Bridwell, L. C. Northcliffe, and S. Datz, Phys. Rev. 176, 427 (1968).
[35]A. B. Wittkower and H. D. Betz, J. Phys. B 4, 1173 (1971).
[36]S. Datz, H. O. Lutz, L. B. Bridwell, C. D. Moak, H. D. Betz, and L. D. Ellsworth, Phys. Rev. A 2, 430 (1970).
[37]T. Tonuma, I. Khono, Y. Miyazawa, F. Yoshida, T. Karasawa, T. Takahashi, and S. Konno, J. Phys. Soc. Jpn. 34, 148 (1973).
[38]R. E. Olson and A. Salop, Phys. Rev. A 16, 531 (1977).
[39]D. W. Rule and K. Omidvar, Astrophys. J. 229, 1198 (1979).
[40]V. S. Nikolaev, Zh. Eksp. Teor. Fiz. 51, 1263 (1966) [Sov. Phys.—JETP 24, 847 (1967)].
[41]K. Omidvar, J. E. Golden, J. H. McGuire, and L. Weaver, Phys. Rev. A 13, 500 (1976).
[42]F. T. Chan and J. Eichler, Phys. Rev. Lett. 42, 58 (1979); Phys. Rev. A 20, 104 (1979); 20, 1841 (1979).
[43]H. Ryufuku and T. Watanabe, Phys. Rev. A 18, 2005 (1978); 19, 1538 (1979); 20, 1828 (1979).
[44]I. S. Dmitriev, Ya. M. Zhileikin, and V. S. Nikolaev, Zh. Eksp. Teor. Fiz. 49, 500 (1965) [Sov. Phys.—JETP 22, 352 (1966)].
[45]V. S. Nikolaev, V. S. Senashenko, and V. Yu. Shafer, J. Phys. B 6, 1779 (1973).
[46]E. Hinnov, Phys. Rev. A 14, 1553 (1976).
[47]J. L. Schwob, M. Klapisch, N. Schweitzer, M. Finkenthal, C. Breton, C. de Michelis, and N. Mattioli, Phys. Lett. 62A, 85 (1977).
[48]E. Hinnov and M. Mattioli, Phys. Lett. 66A, 109 (1978).
[49]J. P. Girard, D. A. Marty, and P. Moriette, IAEA-CN-33/A 17, in *Plasma Physics and Controlled Nuclear Fusion Research* (IAEA, Vienna, 1975), p. 681.
[50]L. C. Northcliffe and R. F. Schilling, Nucl. Data Tables A 7, 233 (1970).
[51]M. I. Green, C. G. Dolo, T. F. Henderson, and D. H. Nelson, IEEE Trans. Nucl. Sci. NS-26, 4003 (1979).
[52]S. K. Allison, Phys. Rev. 109, 76 (1958); S. K. Allison and M. Garcia-Munoz, in *Atomic and Molecular Processes*, edited by D. R. Bates (Academic, New York, 1962).
[53]Yu. A. Tashaev, I. S. Dmitriev, and V. S. Nikolaev, in *Proceedings of the VIII International Conference on the Physics of Electronic and Atomic Collisions*, edited by B. C. Cobic and M. K. Kurepa (Institute of Physics, Belgrade, Yugoslavia, 1973), p. 793.
[54]T. A. Carlson, C. W. Neston, Jr., N. Wasserman, and J. D. McDowell, At. Data 2, 63 (1970).
[55]V. S. Nikolaev (private communication).
[56]P. Moriette, Proceedings of the 7th Yugoslav Symposium on the Physics of Ionized Gases, 1974 (unpublished), p. 43.
[57]D. R. Bates and G. Griffing, Proc. Phys. Soc. London, Sec. A 66, 961 (1953).
[58]E. Merzbacher and H. W. Lewis, in *Encyclopedia of Physics*, edited by S. Flugge (Springer, Berlin, 1958), Vol. 34, p. 166.
[59]A. S. Schlachter, K. H. Berkner, W. G. Graham, R. V. Pyle, P. J. Schneider, K. R. Stalder, J. W. Stearns, J. A. Tanis, and R. E. Olson, Phys. Rev. A (to be published).